Journal of Materials Chemistry A

Accepted Manuscript

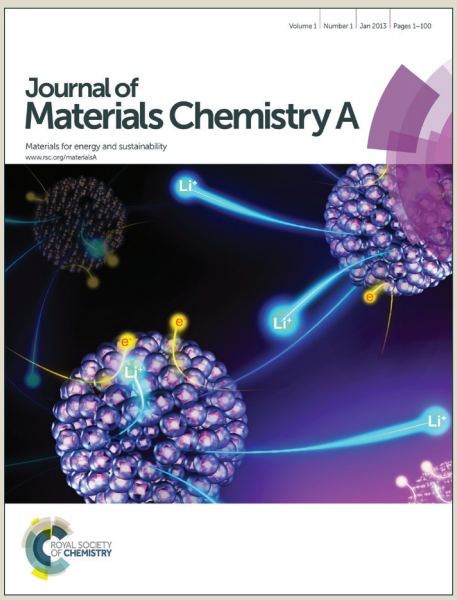

ROYAL SOCIETY OF CHEMISTRY

www.rsc.org/materialsA

Journal of Materials Chemistry A RSCPublishing

ARTICLE

Gas sensing properties of Cd-doped ZnO nanofibers synthesized by electrospinning method

Cite this: DOI: 10.1039/x0xx00000x

Shouli Bai, Song Chen, Yangbo Zhao, Teng Guo, Ruixian Luo,* Dianqing Li,* and Aifan Chen

Received 00th January 2012,
Accepted 00th January 2012

DOI: 10.1039/x0xx00000x

www.rsc.org/

We have used electrospinning followed by thermal treatment to synthesize successfully Cd-doped ZnO nanofibers with different doping concentrations. The research interest is focused on significant enhancement of the sensing performance to CO due to the doping change the state of native defect of the ZnO, which has been confirmed by PL and XPS spectra. The competitive influence of annealing temperature and operating temperature on sensing response of the ZnO was discussed in detail. The sensing mechanism of Cd-doped ZnO sensors on detection of CO was also discussed. In addition, the band structures and densities of states for undoped and Cd-doped ZnO were also calculated using the first-principles based on local density approximation LDA+U scheme. The calculation results show that the band gap is significantly narrowed by doping, which coincide with the results determined from UV-Vis spectra.

1. Introduction

The synthesis and functionalism of metal oxide nanostructures have attracted great interest for the significant potential application.[1] ZnO, a nontoxic, inexpensive and chemically stable n-type semiconductor, has been proved to be an excellent gas sensing material for detection of both toxic and combustible gases. Up to now, one- and two-dimensional nanostructure ZnO with different morphologies and size were rapidly developed. Recently, employing nanoparticles or nanosheets as building blocks self-assembled to 3D micro/nanometer hierarchical structures have caused great interest due to their large surface area and porous structure that beneficial to gas adsorption and diffusion. They are able to provide more promising sensing properties than the conventional bulk counterpart, meanwhile maintaining good chemical and thermal stabilities. To our best knowledge, many techniques such as hydrothermal, ultrasonic irradiation, electrospinning, sol-gel, solid-state chemical reaction, thermal evaporation, chemical vapor deposition, etc. have been used to synthesize different nanostructural ZnO.[2-4] Among them, the hydrothermal method is conventionally recognized to be a convenient method for the preparation of ZnO nanocrystals，the autogenerated pressure from water upon heating can further enhance the solubility and the reactivity of the reactants to improve the crystallinity of the prepared nanocrystals. But the conventional hydrothermal reaction required higher temperature and longer reaction times to produce well morphology metal oxides. The electrospinning technology reported herein has been investigated relatively recently in comparison to other techniques due to its versatility, high-efficiency and low cost operation for preparing organic and inorganic nanofibers that have long lengths, uniform diameters and various compositions.[5]

At present, there are many literatures and experimental works about Cd-doped ZnO. Some of them are about the light-emitting diode (LED) applications, for example, Lupan and Pauporte *et al*. reported the electroluminescence emission wavelength could be tailored by Cd doped ZnO-NRs/p-GaN.[6, 7] Others are related to sensing properties toward different gases. Patil *et al*. studied gas sensing properties of $Zn_{0.9}Cd_{0.1}O$ to LPG, ethanol and acetone, and obtained that the $Zn_{0.9}Cd_{0.1}O$ material could be a candidates for acetone sensors.[8] Lupan *et al*. also reported that Cd-ZnO nanowires exhibited highly sensitive and selective for hydrogen.[9] However, there are not studies on CO sensors based on Cd-doped ZnO. In order to develop a new application of Cd-doped ZnO, in the present study, an *in situ* added cadmium salt during electrospinning process to prepare Cd doped-ZnO nanofibers was performed. The effect of the doping amount on gas sensing was also investigated. The key factor influencing gas response along with the associated sensing mechanism was exposed by PL and XPS analysis. The band and electronic structures of doped-ZnO were calculated by the first-principles, it is coincident with the results obtained by UV-vis measurement and sensing test. This work can give rise to interesting option for researching other metal oxides.

2. Experimental Section

2.1 Preparation of Cd-doped ZnO nanofibers

All the chemicals were analytical grade and used as received without further purification. Cd-doped ZnO nanofibers were synthesized by an electrospinning method and followed by annealing. In a typical procedure, 0.5 g of zinc acetate and certain amount of cadmium nitrate (Cd/ZnO = 0.0, 3.0, 5.0, and 7.0 wt%) were added into 3 mL of N, N-dimethylformamide (DMF) under vigorous stirring for 3 h. Subsequently, 0.6 g of poly (vinylpyrroridone) (PVP, *M*w = 1 300 000) was dissolved into 4 mL ethanol under vigorous stirring for 3 h and both were mixed together under vigorous stirring for 3h. The precursor then introduced into a 20 mL plastic syringe with a metallic needle of 1 mm inner diameter for electrospinning.

A high voltage of 18 kV was supplied at the metallic needle by a DC power supply by a peristaltic pump. A piece of grounded aluminum foil was placed 20 cm below the tip of the needle to collect the nanofibers. The solution jet solidified with accompanying evaporation of solvent at a constant flow rate of 0.4 mL/h. and formed continuous fibers on the collector. Thus, the electrospinning process offers a simplified technique for fiber formatiom. In order to identify the optimum annealing temperature of doped samples, pure ZnO nanofibers was annealed at 400°C, 500°C, 600°C and 700°C for 4 h, respectively. The heating rate was 10°C/min. The optimum annealing temperature of doped samples was selected as the temperature at which the response of pure ZnO was the highest.[10] The pure and Cd-doped ZnO nanocrystals was also prepared by a conventional hydrothermal method[11] and annealed at same temperature of 600°C for 4 h in air to compare their response.

2.2 Characterization

The crystal structure of the Cd-doped ZnO samples was analyzed by X-ray diffraction (Shimadzu XRD-600 diffractometer) analysis, operated at 45 kV and 40 mA using Ni-filtered Cu Kα1 radiation(λ= 0.15406 nm), with a scanning speed of 10o min−1 for 2θ in a range from 20o to 80o. The surface morphology of the electrospun samples was observed using a Hitachi field emission scanning electron microscope (FE-SEM) equipped with an energy dispersive X-ray (EDX) system for chemical composition analysis. PL spectra were recorded from 350 to 600 nm at room temperature by a 325 nm excitation (RF-5301PC spectrometer). Surface elemental analysis was performed using an ESCALAB250 X-ray photoelectron spectroscopy (XPS). UV-Vis absorption spectra of the products were recorded on a Hitachi UV-3010 visible spectrophotometer (Tokyo, Japan), employing distilled water as the reference.

2.3 Sensor fabrication and response measurement

The sensors based on Cd-doped ZnO nanofibers annealed at 600°C for 4 h were fabricated and the responses were measured by monitoring resistance change of the sensor in a temperature-controllable flowing system. The annealed powder was pressed into a pellet with a diameter of 8.0 mm and a thickness of 0.5 mm under a pressure of 7 MPa and a pair of platinum filament was attached on both sides of the pellet to form the sensing element. Then the sensing element was placed in a response test apparatus and pretreated at 320ºC for 3 h to remove the adsorbents on the surface of the sensor. The target gas and air were introduced through two flow meters, respectively, to control the concentration of the target gas. Response measurement was carried out in the temperature range from 55°C to 410°C by adjusting the temperature controller of the heating. For the sensor of semiconductor metal oxide, the resistance was monitored as a function of the gas concentration. When air and ppm-level target gas flowed through the sensor element, the corresponding steady-state resistance of the sensor in air (R_{air}) and in the air–gas mixture (R_{gas}) was recorded, respectively. The response for CO is defined as the ratio of R_{air}/R_{gas}.

3. Results and discussion

3.1 Structure and morphology of pure and Cd-doped ZnO nanofibers

The crystalline structure of the ZnO nanofibers was performed by XRD analysis. Fig. 1 (a) shows the representative XRD patterns obtained from the ZnO nanofibers annealed at different temperatures. The shift in peak position was found to be Δ(2θ) < 0.03° for these samples with respect to the literature values (PDF#36-1451). All of the diffraction peaks of samples can be indexed to the hexagonal wurtzite structure ZnO, and no characteristic peaks of other impurities were observed. This

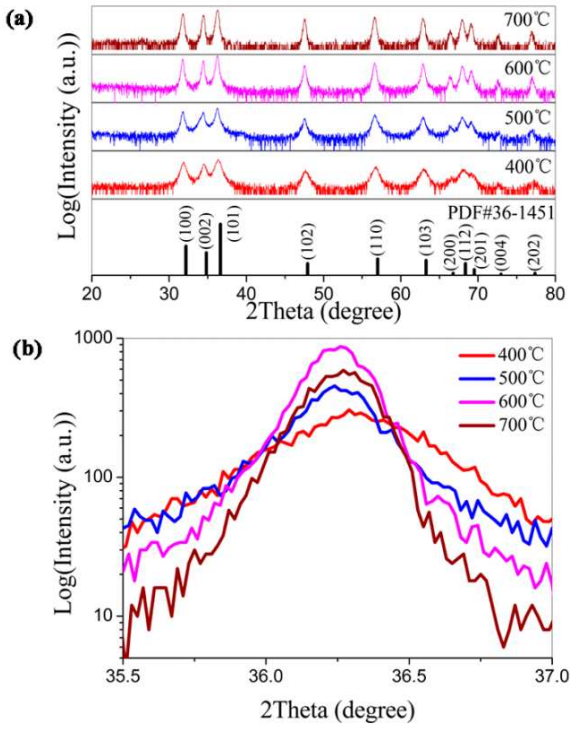

Fig. 1 (a) Representative XRD patterns of ZnO nanofibers calcined at different temperatures and (b) peak profiles of the (1 0 1) diffraction peaks.

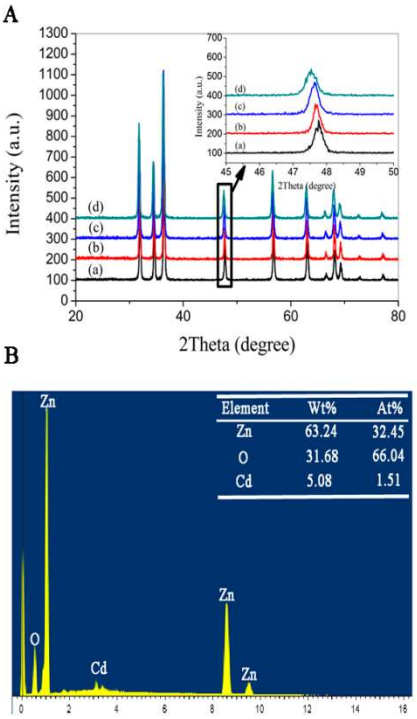

Fig. 2 A XRD patterns of undoped sample (a) and doped samples annealed at 600°C with Cd doping concentration of 3.0 wt% (b), 5.0 wt% (c) and 7.0 wt% (d); top-right corner: a high magnification of the (102) peak; **B** EDX spectrum of 5.0 wt%-Cd doped ZnO sample annealed at 600°C.

suggests that all of the nanofibers contained a single phase of ZnO. In an effort to evaluate the structural perfection, i.e., the crystallinity, the peak intensities of the (1 0 1) Bragg reflections were compared, as shown in Fig. 1 (b). It is to be noted that the (1 0 1) peaks are chosen for comparison because they show the maximum intensity in the diffraction patterns. In general, the intensity of a peak in the XRD pattern reflects the total scattering from the crystal structure of each plane and is directly dependent on the distribution of specific atoms in the structure. Thus, the peak intensity is ultimately related to both the structure and composition of a specific phase. As is summarized in Fig. 1 (b), when the annealing temperature was increased to 600°C, the degree of structural perfection, which is denoted as the peak intensity, also increased. Further increase in the annealing temperature to values over 600°C resulted in a deterioration in the degree of structural perfection.

The doped ZnO annealed at 600°C was also analyzed by XRD. As shown in Fig. 2A (b)-(d), the XRD results show the shift in peak position. The shift in peak position is found to be $\Delta(2\theta) \sim 0.07^{\circ}$, 0.13° and 0.23° for 3.0 wt%, 5.0 wt% and 7.0 wt%-Cd doped ZnO, respectively, with respect to undoped ZnO annealed at 600°C (Fig. 2A (a)). This reveals the change in lattice parameters and cell volumes of Cd-doped ZnO with the change of Cd doping amount. The lattice volume expansion is due to the larger ionic radius of Cd^{2+} (0.97 Å) versus the Zn^{2+} ion (0.74 Å), when Cd^{2+} replaces Zn^{2+} in the ZnO crystal lattice. There are no peaks of the secondary phase (CdO) in the pattern, because the amount is too small to be detected by the XRD. To further prove the existence of Cd component in Cd-doped ZnO, EDX was used to observe the element composition of the sample and the spectrum is illustrated in Fig. 2B, which reveals the presence of Cd, Zn and O and the concentration of Cd is about 5.08 wt% corresponding to Cd doping concentration of 5.0 wt%.

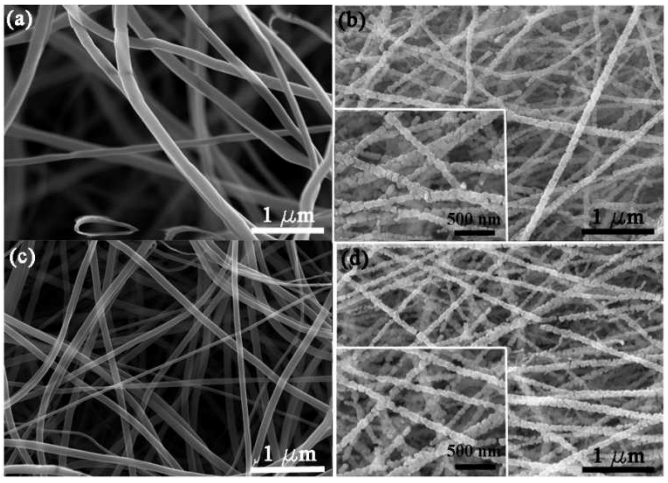

Fig. 3 SEM images of nanofibers: (a) undoped ZnO/PVP nanofibers. (b) undoped ZnO nanofibers annealed at 600°C. (c) 5.0 wt%-Cd doped ZnO/PVP nanofibers and (d) 5.0 wt% Cd-doped ZnO nanofibers annealed at 600°C

The morphology of the electrospinning nanofibers was studied by scanning electron microscopy (SEM). Fig. 3 shows the SEM images of as-synthesized undoped ZnO/PVP and 5.0 wt%-Cd doped ZnO/PVP nanofibers before and after annealing. In both cases, the samples are composed of uniform nanofibers free of beads. Moreover, the distributions of nanofibers are fairly random with no distinct alignment owing to the bending instability associated with the spinning jet. From Fig. 3 (a) and (c), the as-synthesized undoped and Cd-doped ZnO/PVP nanofibers before annealing have smooth surface because of amorphous ZnO/PVP and polymeric property. They are long than several millimeters, with a diameter of approximate 200 nm. Furthermore, it can be seen that, in contrast to undoped ZnO/PVP nanofibers, the diameter of Cd-doped ZnO/PVP nanofibers slightly decreases. This may be due to introduction of $Cd(NO_3)_2$, which altered the conductivity and viscosity of the precursor solution, leading to thinner diameters of Cd-doped ZnO/PVP nanofibers.[12] After annealing of 600°C, the diameters of undoped and Cd-doped ZnO nanofibers shrank to approximate 100 nm, as shown in Fig. 3 (b) and (d). The shrinkage of nanofibers is due to the removal of PVP from the fibers and the conversion of metal salts to metal oxides. It can also be seen from the inset images of Fig. 3 (b) and (d) that the surface of undoped and Cd-doped ZnO nanofibers has been laterally cut into chains composed by nanoparticles appearing a rough porous structure.

3.2 The effect of annealing temperature on particle size and specific surface of ZnO nanofibers

The effect of the annealing temperature on sensing response originally resulted from the particle size and crystallinity. The

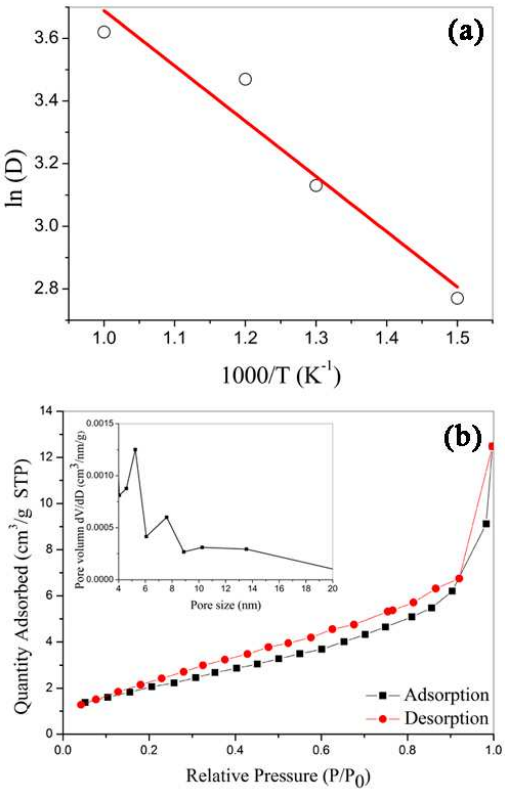

Fig. 4 (a) Plot of ln D versus 1/T; the slope furnishes the activation energy for particle growth and (b) Nitrogen adsorption-desorption isotherms at ZnO nanofibers calcined at 400°C, inset is pore size distribution images.

particle size and crystallinity of ZnO nanofibers are related to the annealing temperature of the sample by XRD analysis. It is known that the dependence between particle size and annealing temperature obeys the Arrhenius equation, $D = A*\exp(-E_a/RT)$, where D is the average grain size, A is the pre-exponential factor, E_a is the apparent activation energy for particle growth, R is the gas constant, and T is temperature (in K). Fig. 4 (a) shows the plot of ln D as a function of 1/T (in K^{-1}) and the apparent activation energy estimated from the slopes is 14.67 kJ/mol. The driving force for the particle growth is the reduction in the free energy of the system caused by a reduction in the total particle boundary area.

The effect of annealing temperature on the surface areas of ZnO nanofibers was investigated by means of Brunauer-Emmett-Teller (BET) analysis. The surface areas of samples annealed at different temperatures were measured by nitrogen adsorption and desorption isotherm techniques. The BET analysis shows that the surface area are 27.8 m^2/g, 18.5 m^2/g and 16.9 m^2/g corresponding to different annealing temperatures of 400°C, 500°C and 600°C, respectively. We found the surface area decreases with the increase of annealing temperature. Moreover, the ZnO nanofibers annealed at 400°C shows a type IV isotherm with type H3 hysteresis loops (Fig. 4 (b)), which exhibits three features as follows: It belongs to multilayer adsorption; H3 type isotherms does not exhibits capillary condensation in microspheres; Adsorption heat of the first layer

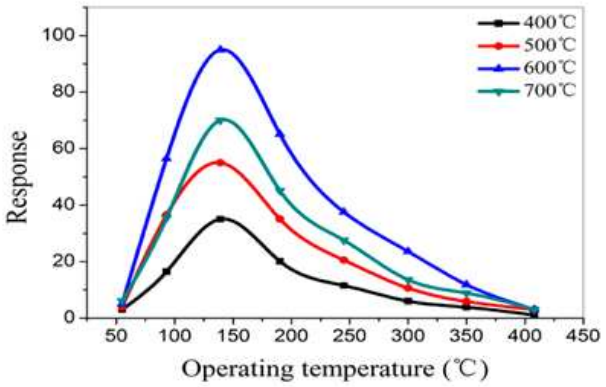

Fig. 5 A Responses of ZnO nanofibers annealed at different temperatures to 40 ppm CO.

is smaller than condensation heat of the medium. The pore size distribution (PSD, Fig. 4 (b) inset) curves were derived by the Barret-Joyner-Halenda (BJH) method, which reveal a bimodal and narrow pore size distribution centred at about 5.2 nm in the sample annealed at 400°C.

3.3 Effects of operating temperature, annealing temperature and doping on sensing properties of ZnO sensors

Fig. 5A presents the typical response characteristics of pure ZnO nanofibers to 40 ppm CO as a function of operating temperature at different annealing temperatures. Many reports have demonstrated that the response of a semiconductor sensing material is greatly affected by operating temperature. The change of operating temperature alters the kinetics of the oxygen adsorption and reactions of the gases adsorbed on sensor surface, leading to the alteration of material resistance.[13] The response increases with operating temperature as the temperature range from 55°C to 135°C due to sufficient thermal energy is essential to overcome the activation energy barrier of chemisorption and surface reaction. The response of the sample

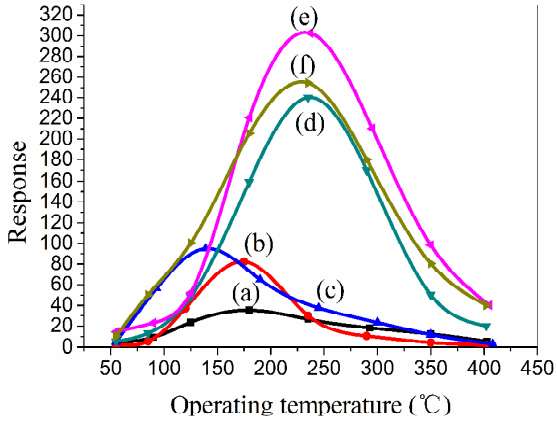

Fig. 6 Responses of Cd-doped ZnO nanorods (Hydrothermal synthesis) with different doping amount (0.0 wt% (a) and 5.0 wt% (b)) and Cd-doped ZnO nanofibers (Electrospun) with different doping amount (0.0 wt% (c), 3.0 wt% (d), 5.0 wt% (e) and 7.0 wt% (f)) calcined at 600°C to 40 ppm CO.

Table 1 Response to CO of Cd-doped ZnO nanofibers reported in this work compared to other-doped ZnO sensing materials reported in literatures

Sample	Cd-doped ZnO nanofibers	Mg-doped ZnO nanowires	Cu-doped ZnO thin films
Response	300	111	2.7
CO concentration (ppm)	40	50	20
Reference	this work	15	16
Sample	Au-doped ZnO nanorods	Co-doped ZnO nanorods	Pd-doped ZnO nanofibers
Response	12	8.2	5.5
CO concentration (ppm)	1000	50	20
Reference	17	18	19

annealed at 600°C reaches a maximum value of 95 at operating temperature of 135°C. The temperature at which the response exhibits a maximum value is called the optimum operation temperature. However, if the operating temperature was further increased above 135°C, the response decreases because the amount of adsorbed gas on the material surface will decrease, while the desorption process becomes dominant with increasing operating temperature, leading to the decrease in response. When desorption rate of the gas equal to that of adsorption, the maximum loading of chemisorbed ions is reached at the optimum temperature, resulting in the highest response.

In addition to surface area the crystallinity of the particles existing in individual nanofibers need to be optimized to obtain the best sensing properties (Fig. 5A), because both is competitively influencing the sensing properties. If the annealing temperature is lower, although the specific surface is larger, the crystallinity does not satisfy the requirement for sensor application. If the annealing temperature is too high, the specific surface is significantly decreased, leading to decrease of gas response. From test results the annealing temperature of 600°C is found to be the appropriate annealing temperature for ZnO nanostructures, at which the response reached the highest since the crystallinity becomes better while the specific surface without dramatically decreases.

Doping has been early proved to be a facile and efficient method to improve the sensing property of semiconductor sensors because doping can effectively modulates the parameters of crystal cell and band structures of ZnO nanocrystals. The responses to CO of samples doped with different Cd concentrations of 0.0 wt%, 3.0 wt%, 5.0 wt% and 7.0 wt% were shown in Fig. 6 (c)-(f), respectively. It can be seen that the response of 5.0 wt%-Cd doped ZnO sample is up

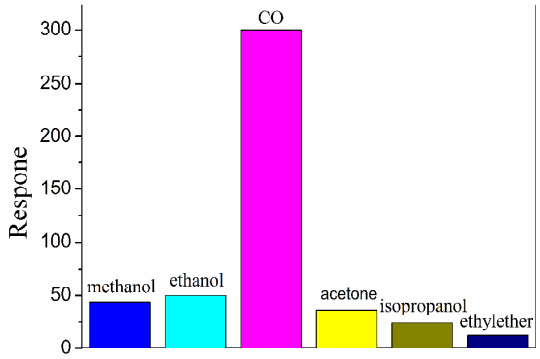

Fig. 7 Responses of 5.0 wt%-Cd doped ZnO nanofibers annealed at 600°C to 40 ppm different gases.

to 300 as exposed to 40 ppm CO at operating temperature of 235°C, which is about 3 times higher than that of undoped sample. While the responses of 3.0 wt%- and 7.0 wt%-Cd doped samples are lower than that of 5.0 wt% doped sample except former both operated at a higher temperature to obtain comparable response with latter. Comparison with the electrospinning technology, the responses of the samples synthesized using hydrothermal method[14] is lower at same conditions as shown in Fig. 6 (a) and (b). Besides, comparing with the maximum responses reported in literature, Cd-doped ZnO nanofibers synthesized in the work exhibits excellent response to CO and these data have been cited in Table 1. As shown in Fig. 7, Cd-doped ZnO nanofibers also exhibit excellent selectivity.

3.4 Key factor influencing sensing performance of undoped and doped ZnO nanofibers

In order to analyze the key factor influencing sensing performance of undoped and doped ZnO sensing material, the native defects of them were studied in detail by room temperature photoluminescence measurement which is an effective way to study the defect structure of the semiconductor metal oxides.[20] As there are primarily two kinds of defects: the donor (DL) and the acceptor (AL), therefore we tried to decompose the PL spectra to distinguish the DL and AL subpeaks. It is generally believed to be six intrinsic defects in ZnO: interstitial zinc (Zn_i), zinc vacancy (V_{Zn}), oxygen vacancy (V_O), oxygen interstitial (O_i), oxygen antisite (O_{Zn}) and Zn antisite (Zn_O).[21] Of the six defects, Zn_O are unlikely to be stable under equilibrium conditions due to their high formation energies even at rich Zn atmosphere; Zn_i and V_O are donors that give rise to free electrons, while V_{Zn}, O_i and O_{Zn} are acceptors that consume free electrons.[22] To investigate relative content

between donors and acceptors for undoped and Cd-doped ZnO the photoluminescence measurement was carried out at room temperature by exciting the sample with a He-Cd laser at 325nm. Fig. 8 (a) presents the room temperature photoluminescence spectra of undoped and Cd-doped ZnO, and

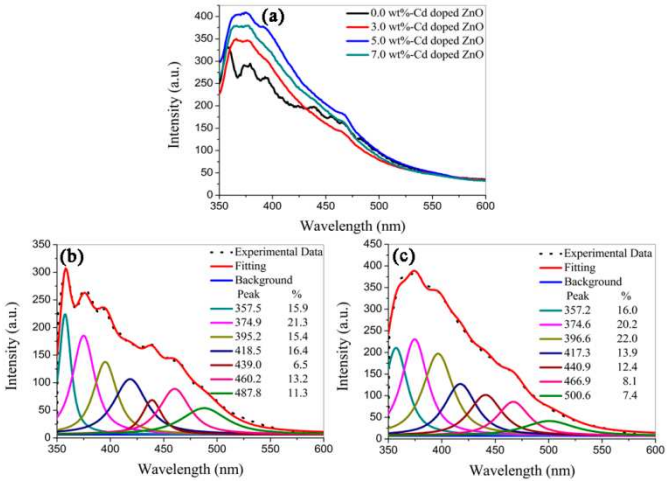

Fig. 8. Room temperature photoluminescence spectra of undoped and Cd-doped ZnO calcined at 600°C (a); Gaussian deconvolutions of the PL spectra of undoped ZnO sample (b) and 5.0 wt%-Cd doped ZnO sample (c).

Fig. 8 (b) and (c) present the defect-related luminescence and Gaussian deconvolutions of the PL spectra for undoped and 5.0 wt%-Cd doped ZnO. The percentages of donors and acceptors can be obtained by peak separation from Fig. 8 (b) and (c), and it is found that the content of donors for undoped ZnO is 49.6%. Moreover, Fig. 8 (c) presents deconvolution of the PL peak for 5.0 wt%-Cd doped ZnO sample, which reveals seven PL peaks centred at 357, 374, 397, 417, 440, 467, 501 nm, respectively. According to their origin, in the UV emission region (shown in Fig. 8 (c)), the peaks located to 357 nm and 374 nm with the corresponding energy of 3.3-3.4 eV are called as near band edge emission (NBE), which result from the recombination of electrons in the conduction band and holes in the valence band. The peak centred at 397 nm can be assigned to one of the shallow donor level, which could not be excited to the conduction band because some excited electrons lose energy through phonon emission;[23] both peaks of 417 and 440 nm are attributed to Zn_i;[24] the peak centred at 467 nm is related to V_{Zn}; the peak of 501 nm is attributed to V_O.[25] Summarily, the percentages of donors (Zn_i and V_O) and acceptors (V_{Zn}, O_i and O_{Zn}) can be obtained by peak separation from Fig. 8 (c), and it is found that 5.0 wt%-Cd doped ZnO has the higher donors content (55.7%) than that of undoped sample. More donors in ZnO sample is beneficial to the adsorption of oxygen and surface reaction, so the response is significantly enhanced by doping 5.0 wt%-Cd.

3.5 Transient response and nonlinear fit for Cd-doped ZnO based sensors

To investigate the time dependence of response, Fig. 9 shows the transient responses of the undoped and Cd-doped ZnO based sensors to different CO concentrations (20, 40 and 60 ppm). It is found that the response has been enhanced by Cd doping and also indicated the time dependence of the electrical resistance in measurement of response. The response time and recovery time of the sensor were measured as the time taken for

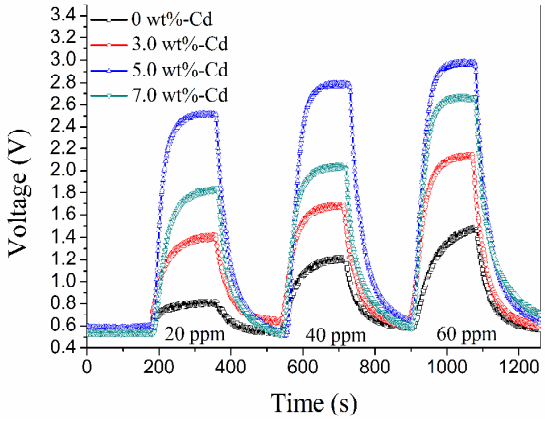

Fig. 9 Transient responses of sensors based on undoped and different concentrations Cd-doped ZnO to different ppm CO.

the sensor output to reach 90% of the highest response. The response time and the recovery time are about 10 s and 27 s, respectively. It can be concluded that the Cd-doped ZnO nanofibers synthesized by electrospinning is a promising sensing material for CO sensor. As shown in Fig. 9, the original base resistance is not recovered fully (at least within the similar time scale of the response transient) by turning off the test gas and flushing with air. So, the sensing transients are termed to irreversible. For the irreversible gas sensing, the surface reaction can be explained by Langmuir-Hinshelwood reaction mechanism and the response transient (S (t)) can be expressed by Eq. (1):[26]

$$S(t) = S_{max}\left(1-\exp^{-[t/\tau_{irrev}]}\right) \quad (1)$$

Where $\tau_{irrev} = 1/(k * C_g)$ (k-rate constant; C_g-gas concentration) τ is referred as characteristic response time for the gas sensing of irreversible type. Respective response transients for CO concentrations in 20, 40 and 60 ppm were fitted nonlinearly according to Eq. (1) and the fitted results show that the characteristic response time is reduced disproportionately with the increase of the CO concentration for the gas sensor of irreversible type.

3.6 Sensing mechanism of Cd-doped ZnO sensors to CO

It is known that metal oxide gas sensing depends on the interaction between the test gas and the adsorbed oxygen (O^- and O^{-2}) ions on the surface of the material. When the ZnO nanofibers was exposed in air atmosphere, oxygen molecules will adsorb on the nanofibers surface and capture electrons from ZnO to generate chemisorbed oxygen species of O^{-1} and O^{-2} at higher temperature, leading to the increase of resistance.

$$O_{2\,(gas)} \rightarrow O_{2\,(ads)} \quad (2)$$

$$O_{2\,(ads)} + 2e^- \rightarrow 2O^-_{\,(ads)} \quad (3)$$

$$1/2\ O_{2(ads)} + 2e^- \rightarrow O^{-2}_{\,(ads)} \quad (4)$$

When the ZnO nanofibers was exposed to the CO atmosphere, the exchange of charges between the CO and the oxygen species adsorbed on ZnO surface caused the variation of the charge depletion layer, that is, the variation of the surface barrier height for electrons in the conduction band, which is different with different doping Cd concentration. The electrons will be released to the conduction band with CO oxidizing, and the resistance of nanofibers will reduces through following reactions:

$$CO_{(gas)} + O^-_{(ads)} \rightarrow CO_2 + e^- \quad (5)$$

$$CO_{(gas)} + O^{-2}_{(ads)} \rightarrow CO_2 + 2e^- \quad (6)$$

Lupan et al. reported that the higher gas response of single nanowire compared with thin film is mainly due to a larger surface-to-volume ratio and a more effective modulation of the surface depletion layer in individual ZnO nanowire. ZnO nanofibers synthesized in the work possesses large surface-to-volume ratio, which can adsorb more target gas molecules and more surface atoms will participate in surface reactions. Thus, one way to improve gas response is to increase the surface/volume ratio. Another component of influencing gas response is related to the change of defects, especially oxygen vacancies, can influence the electronic/chemical properties, adsorption behaviour and reversibility of sensor characteristics. Cd doping can change the state of native defects as analysed in above PL spectra, which induces an increase of the carrier concentration in doping ZnO, leading to the change of response characteristics as shown in following:

$$CO + Oo^X \rightarrow CO_2 + V^{\cdot\cdot} + 2e \quad (7)$$

Where Oo^X is neutral oxygen in oxygen site, $V^{\cdot\cdot}$ is double positive charged oxygen vacancies; e is negatively charged electron according to the Kro¨ger–Vink notation.[27, 28] XPS analysis was conducted to confirm the change of ZnO defects due to Cd doping and Cd chemical state in the ZnO matrix. Fig. 10 shows high-resolution XPS spectra of Zn 2p, O 1s and Cd 3d for the undoped and Cd-doped ZnO. In Fig. 10 (b) spectrum, only C, Zn， O and Cd related core levels are detectable, indicating that no impurities are introduced. In Fig. 10 (c), the Zn 2p peaks of binding energy for undoped ZnO are observed at 1021.8 and 1044.8 eV, respectively corresponding to the spin-orbit of Zn $2p_{3/2}$ and Zn $2p_{1/2}$, which suggests that Zn in the samples only exists in a divalent-oxidation state.
Furthermore, the binding energies for the Cd-doped ZnO samples increase 0.7 eV compared with the undoped ZnO sample (from 1021.8 eV to 1022.5 eV for Zn $2p_{3/2}$ and from 1044.8 eV to 1045.5 eV for Zn$2p_{1/2}$). The shifts in binding energies reflect the electronic interaction between the ZnO and dopant, which is responsible for the enhancement of gas response for the Cd-doped ZnO.[29] As shown in Fig. 10 (d), the main peaks observed at 405.4 and 412.2 eV correspond to the binding energy of Cd $3d_{3/2}$ and $3d_{1/2}$, respectively. Fig. 10 (e) and (f) present the Gauss fitting curves of O 1s spectra of

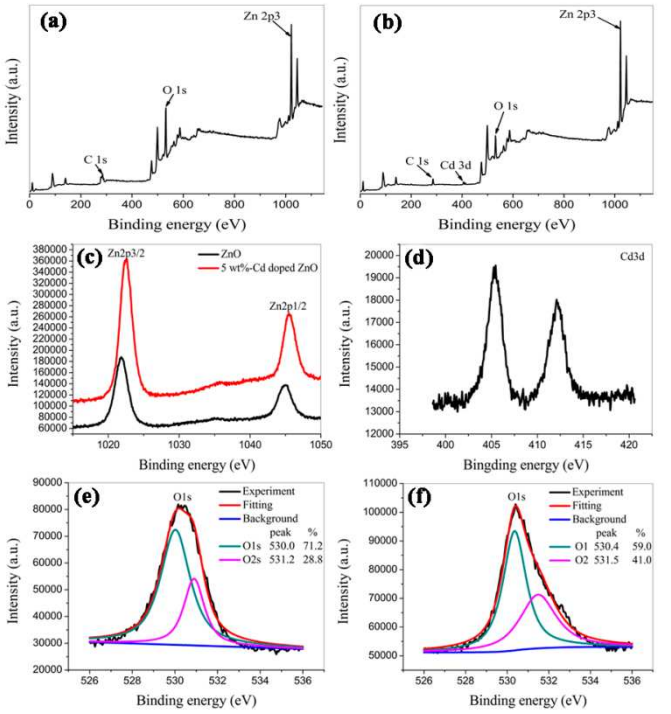

Fig. 10 (a) and (b) XPS spectra of undoped and 5.0 wt%-Cd doped ZnO; (c) Zn region of undoped and 5.0 wt%-Cd doped ZnO; (d) Cd region; (e) and (f) O region for undoped and 5.0 wt%-Cd doped ZnO samples, respectively.

undoped ZnO and 5.0 wt% Cd-doped ZnO. Two species centred at ~530.0 eV (O1) and ~531.0 eV (O2) are indexed. The main species of O1 on the lower binding energy side of the O 1s spectrum are perhaps attributed to the coordination of oxygen in Zn-O. While the higher binding energy species of O2, centered at 531.0, belong to O^- and O^{2-} ions in the oxygen-deficient region caused by oxygen vacancies.[30] It is obvious that Cd-doped ZnO have more donor content(such as the oxygen vacancies)than undoped ZnO. The analysis results indicate that the Cd doping can modify the surface state of ZnO, leading to the enhancement of gas sensing. Thus, we can draw a conclusion that the intrinsic characteristic in enhancing gas sensing results from the changes of defects (i.e. nonstoichiometry) and electronic binding energy in ZnO, which can be attributed to chemical and electronic synergistic effects between the components in material.

4. First principle calculations based on density functional theory

Based on the data obtained from XRD and EDX, the 1×1×1 unit cell of pure ZnO (Fig. 11a) and the different supercells formed by one Cd atom substituted one Zn atom as shown in

Fig.11 (b)-(d) were used. All calculations were performed with the Material Studio, which is based on the density functional theory using the plane-wave ultrasoft pseudo-potential method to explore the change trend of band gap with increasing Cd doping concentration. The generalized gradient approximation (GGA) in the scheme of Perdew-Burke-Ernzerhof was used to

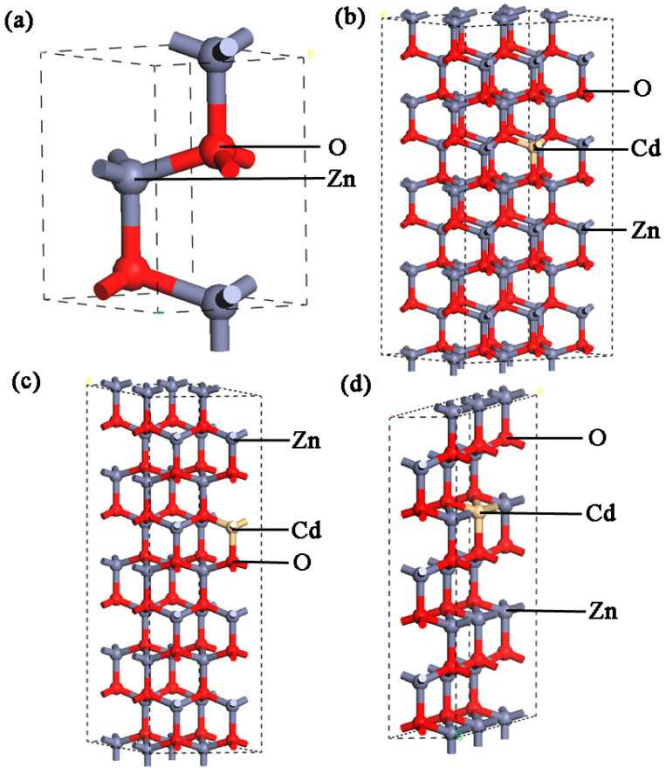

Fig. 11 (a) 1×1×1 unit cell of undoped ZnO, (b) 2×3×4 supercell of $Zn_{0.9792}Cd_{0.0208}O$, (c) 2×2×4 supercell of $Zn_{0.9688}Cd_{0.0313}O$ and (d) 1×3×3 supercell of $Zn_{0.9444}Cd_{0.0556}O$.

treat the exchange-correlation function.[31] The cut-off energy for the plane wave expansion was set to 340 eV.

For the Brillouin zone integration, we used a 9×9×6 k-point Monkhorst-pack mesh for the unit cell of pure ZnO, a 4×3×1 k-point Monkhorst-pack mesh for the supercell of $Zn_{0.9792}Cd_{0.0208}O$, a 4×4×1 k-point Monkhorst-pack mesh for the supercell of $Zn_{0.9688}Cd_{0.0313}O$ and a 9×3×2 k-point

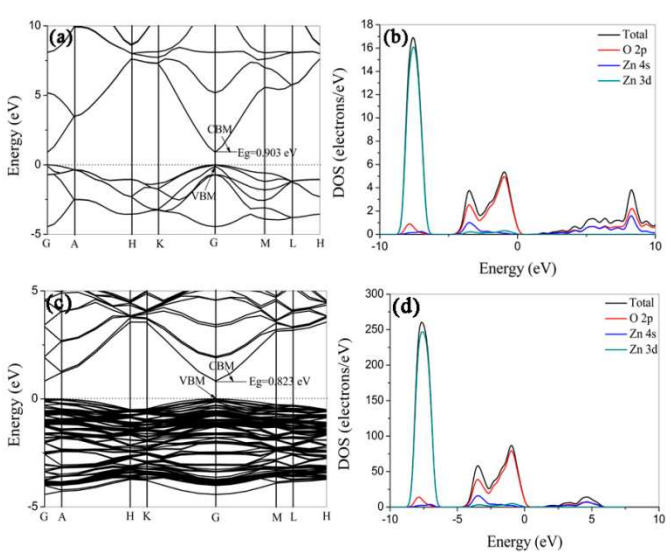

Fig. 12 (a) Band structure of the unit cell of undoped ZnO, (b) TDOS and PDOS of the unit cell of undoped ZnO, (c) Band structure of the unit cell of 5.0 wt%-Cd doped ZnO and (d) TDOS and PDOS of the unit cell of 5.0 wt%-Cd doped ZnO.

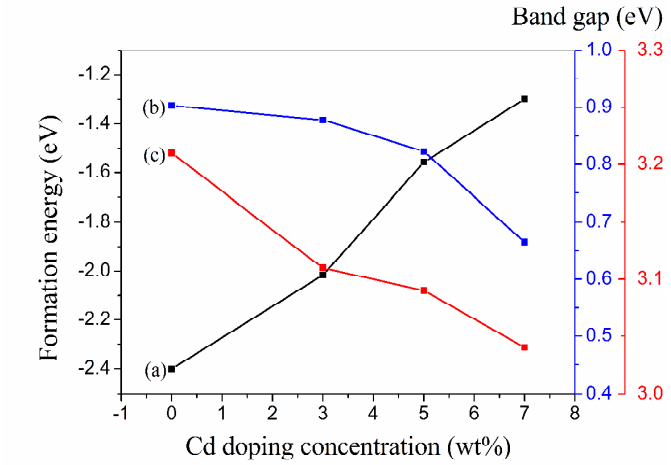

Fig. 13 Calculated formation energy E_f (a), calculated band gap E_g (b) and band gap E_g (c) obtained from UV-Vis absorption spectra for undoped and Cd-doped ZnO nanofibers.

Monkhorst-pack mesh for the supercell of $Zn_{0.9444}Cd_{0.0556}O$. In the optimization process, the energy change and the maximum tolerances of the force, stress, and displacement were set to 1×10^{-5} eV/atom, 0.3 eV/nm, 0.05 Gpa and 1.0×10^{-4} nm, respectively.[32]

Fig. 12 (a) and (b) show the band structure (BS), total density of states (TDOS) and partial density of states (PDOS) of the unit cell of pure ZnO, respectively. As shown in Fig. 12 (a), the calculated band gap (E_g) of pure ZnO is 0.903 eV, which is close to the previously calculated value.[33] Although the calculated value is always less than the experimental value due to the limitation of DFT in GGA, the discrepancy does not influence the analysis of the relative value in electronic structures of pure vs. doped ZnO. As shown in Fig. 12 (b), the valence band (VB) of ZnO is formed by the Zn-3d states and O-2p states, and the conduction band (CB) is mainly formed by

the Zn-4s states and O-2p states. The BS, TDOS and PDOS of 5.0 wt%-Cd doped ZnO were shown in Fig. 12 (c) and (d), respectively. From Fig.12(c), the valence band maximum and the conduction band minimum located at the same G point, indicating that the ZnO is a direct band gap semiconductor. We also find that the band gap of 5.0 wt%-Cd doped ZnO becomes narrower (0.823 eV) due to the CB undergoes a shift toward the low-energy region (Fig. 12(d)), the Fermi energy of 5.0 wt%-Cd doped ZnO obtained by calculating decreases from 2.62 eV to 2.36 eV corresponding to that of undoped ZnO, which cause the metallic behaviour of the ZnO. The relationship between the band gap and the Cd concentration in ZnO was plotted in Fig. 13(b). Additionally, we analyzed the relative degree of difficulty of doping wurtzite ZnO with Cd by comparing impurity formation energies (E_f) using the following formula;[34]

$$E_f = E_{tot}(ZnO+Cd) - E_{tot}(ZnO) - E_{Cd} + E_{Zn} \quad (8)$$

Where $E_{tot}(ZnO+Cd)$ and $E_{tot}(ZnO)$ are the total energies of Cd-doped ZnO and pure ZnO respectively in a supercell of the same size. E_{Cd} and E_{Zn} are the energies of bulk Cd and Zn metal,

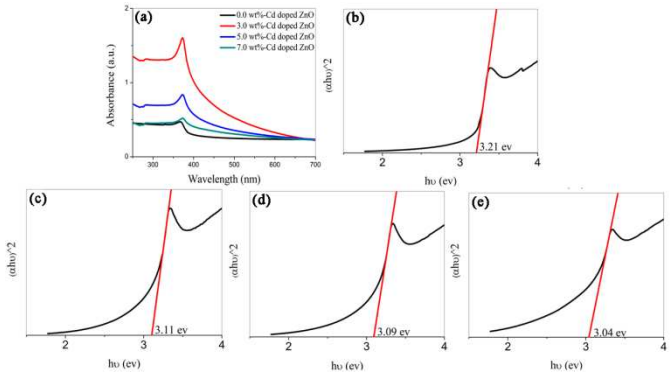

Fig. 14 UV-Vis adsorption spectra of undoped and Cd-doped ZnO calcined at 600°C (a) and plots of $(\alpha h\nu)^2$ *vs* photon energy ($h\nu$) for undoped ZnO (b), 3.0 wt%-Cd doped ZnO (c), 5.0 wt%-Cd doped ZnO (d) and 7.0 wt%-Cd doped ZnO (e).

respectively. The calculated results were shown in Fig. 13(a), find that the E_f increases with increasing Cd concentration in ZnO, which imply doping becomes difficulty and the doping model becomes less stable. So, an appropriate dopant and doping concentration should be considered from two factors of the enhancement of impurity formation energy and the narrowing of the band gap via doping. The band gap values of undoped and Cd-doped ZnO samples were also measured by UV-Vis absorption spectra to compare with the calculated results. As shown in Fig. 14(a), the samples exhibit a strong absorption band at ~370 nm of UV region. Fig. 14 (b)-(e) show plots of $(\alpha h\nu)^2$ *vs* photon energy ($h\nu$) with frequency ν. The direct band gap energy (E_d) can be obtained from Fig. 14 (b)-(e) according to simplified formula $(\alpha h\nu)^2 = C^*(h\nu - E_d)$. Herein α is absorption coefficient and C is a constant.[35] The E_d values corresponding to doping concentration of 0.0, 3.0, 5.0, and 7.0 wt%, were summarized in Fig. 13 (c), and the change trend of band gap is in agreement with that of obtaining by first principle calculations.

5. Conclusion

ZnO nanofibers have been synthesized by electrospinning and annealing of 600°C for 4 h. The response to 40 ppm CO is significantly enhanced from 95 to 300 by 5.0 wt% Cd doping at operation temperature of 235°C. The response and recovery time is about 10 and 27 s, respectively. The characteristic response time is reduced disproportionately with the increase of the CO concentration via modelling transient response using Langmuir-Hinshelwood reaction mechanism. It has been confirmed by PL and XPS that the response enhancement of Cd-doped ZnO are not only related to the increase of donor (oxygen vacancies) content, but also associated with electronic binding energy between the component and dopant in ZnO. The first-principle calculated results show that the band gap is narrowed by Cd doping compared with pure ZnO and that the heavier the Cd concentration is, the narrower the band gap.

Acknowledgements

The work was supported by the National Natural Science Foundation of China (Grant Nos. 21177007 and 51372013), the Dean Project of Guangxi Key Laboratory of Petrochemical Resource Processing and Process Intensification Technology and Beijing Key Laboratory of Environmentally Harmful Chemicals Analysis.

Notes and references

Address here. State Key Laboratory of Chemical Resource Engineering, Beijing University of Chemical Technology, Beijing100029, China. E-mail: luorx@mail.buct.edu.cn

1. G. R. Patzke, Y. Zhou, R. Kontic and F. Conrad, *Angew. Chem. Int. Ed.*, 2010, **49,** 2-36.
2. N. E. Sung, I. J. Lee, A. Thakur, K. H. Chae, H. J. Shin and H. K. Lee, Mater. *Res. Bull.*, 2012, **47**, 2891-2894.
3. F. H. Wang, H. P. Chang, C. C. Tseng, C. C. Huang and H. W. Liu, Curr. *Appl. Phys.*, 2011, **11**, 12-16.
4. Y. H. Zheng, C. Q. Chen, Y. Y. Zhan, X. Y. Lin, Q. Zheng, K. M. Wei and J. F. Zhu, *J. Phys. Chem. C*, 2008, **112**, 10773-10777.
5. A. Greiner and J. H. Wendorff, *Angew. Chem. Int. Ed.*, 2007, **46**, 5670-5703.
6. O. Lupan, T. Pauporte, T. L. Bahers, I. Ciofini and B. Viana, *J. Phys. Chem. C*, 2011, **115**, 14548-14558.
7. T. Pauporte, O. Lupan and B. Viana, Phys. *Status Solidi A*, 2012, **209**, 359-363.
8. J. Y. Patil, A. V. Rajgure, L. K. Bagal, R. C. Pawar, I. S. Mulla and S. S. Suryavanshi, *Ceram. Int.*, 2013, **39**, 4383-4390.
9. O. Lupan, L. Chow, T. Pauporte, L. K. Ono, B. R. Cuenya and G. Chai, *Sens. Actuators, B*, 2012, **173**, 772-780.
10. S. L. Bai, L. Y. Chen, S. Chen, R. X. Luo, D. Q. Li, A. F. Chen and C. C. Liu, *Sens. Actuators, B*, 2014, **190**, 760-767.
11. Y. Peng, S. C. Qin, W. S. Wang, A. W. Xu, *Cryst. Eng. Comm.* 15 (2013) 6518-6525.

12. M. G. Zhao, X. C. Wang, L. L. Ning, H. He, J. F. Jia, L. W. Zhang and X. J. Li, *J. Alloys Compd.*, 2010, **507**, 97-100.
13. S. L. Bai, J. W. Hu, D. Q. Li, R. X. Luo, A. F. Chen and C. C. Liu, *J. Mater. Chem.*, 2011, **21**, 12288-12294.
14. Y. Peng, S. C. Qin, W. S. Wang and A. W. Xu, *Cryst. Eng. Comm.*, 2013, **15**, 6518-6525.
15. C. H. Jin, S. H. Park, H. Kim, S. An and C. M. Lee, Bull. Korean Chem. Soc., 2012, **33**, 1993-1997.
16. H. Gong, J. Q. Hu, J. H. Wang, C. H. Ong and F. R. Zhu, *Sens. Actuators, B*, 2006, **115**, 247-251.
17. P. Rai, Y. S. Kim, H. M. Song, M. K. Song and Y. T. Yu, *Sens. Actuators, B*, 2012, **165**, 133-142.
18. Y. J. Li, K. M. Li, C. Y. Wang, C. I. Kuo and L. J. Chen, Sens. Actuators, B, 2012, **161**, 734-739.
19. S. H. Wei, Y. Yu and M. H. Zhou, Mater. Lett., 2010, **64**, 2284-2286.
20. C. Richard, A. Catlow, A. A. Sokol and A. Walsh, *Chem. Comm.*, 2011, **47**, 3386-3388.
21. M. D. McCluskey and S. J. Jokela, J. Appl. Phys., 2009, **106**, 071101.
22. X. Q. Wei, B. Y. Man, M. Liu, C. S. Xue, H. Z. Zhuang and C. Yang, *Physica B*, 2007, **388**, 145-152.
23. L. Wang, J. W. Ren, X. H. Liu, G. Z. Lu and Y. Q. Wang, *Mater. Chem. Phys.*, 2011, **127**, 114-119.
24. H. B. Zeng, G. T. Duan, Y. Li, S. K. Yang, X. X. Xu and W. P. Cai, *Adv. Funct. Mater.*, 2010, **20**, 561-572.
25. W. D. Cheng, P. Wu, X. Q. Zou and T. J. Xiao, *Appl. Phys.*, 2006, **100**, 054311.
26. H. B. Zeng, G. T. Duan, Y. Li, S. K. Yang, X. X. Xu and W. P. Cai, *Adv. Funct. Mater.*, 2010, **20**, 561-572.
27. O. Lupan, L. Chow, S. Shishiyanu, E. Monaico, T. Shishiyanu, V.Sontea, B. Roldan Cuenya, A. Naitabdi, S. Park, A. Schulte, *Mater. Res. Bull.*, 2009,44, 63–69
28. O. Lupan, V.V. Ursaki, G. Chai, L. Chow, G.A. Emelchenko, I.M. Tiginyanu, A.N. Gruzintsev, A.N. Redkin，*Sens. Actuators, B*, 2010, 144, 56–66.
29. A. Samariya, R. K. Singhal, S. Kumar, Y. T. Xing, M. Alzamora, S. N. Dolia, U. P. Deshpande, T. Shripathi and E. B. Saitovitch, *Mater. Chem. Phys.*, 2010, **123**, 678-684.
30. M. Chen, Z. H. Wang, D. M. Han, F. B. Gu and G. S. Guo, *J. Phys. Chem. C*, 2011, **115**, 12763-12773.
31. D. G. Guo and C. G. Hu, *App. Surf. Sci.*, 2012, **7**, 6987-6992.
32. Y. Liu, Q. Y. Hou, H. P. Xu, L. M. Li and Y. Zhang, *Physica B*, 2012, **407**, 2359-2364.
33. S. A. Ansari, M. M. Khan, S. Kalathil, A. Nisar, J. Lee and M. H. Cho, *Nanoscale*, 2013, **5**, 9238-9246.
34. X. Y. Cui, J. E. Medvedeva, B. Delley, A. J. Freeman, N. Newman and C. Stampfl, *Phys. Rev. Lett.*, 2005, **95**, 256404.
35. L. Y. Zhang, L. W. Yin, C. X. Wang, N. Lun, Y. X. Qi and D. Xiang, *J. Phys. Chem. C*, 2010, **114**, 9651-9658.

The response of ZnO nanofibers is significantly enhanced *via* Cd doping, which can be attributed to the change of defects in ZnO and has been confirmed by PL and XPS analysis.